Intraoperative Assessment of Tumor Resection Margins in Breast-Conserving Surgery using ^{18}F-FDG Cerenkov Luminescence Imaging – A First-in-Human Feasibility Study

Maarten R. Grootendorst[1,2]

Massimiliano Cariati[1,2]

Sarah E. Pinder[1]

Ashutosh Kothari[2]

Michael Douek[1,2]

Tibor Kovacs[2]

Hisham Hamed[2]

Amit Pawa[3]

Fiona Nimmo[4]

Julie Owen[1]

Vernie Ramalingam[2]

Sweta Sethi[2]

Sanjay Mistry[2]

Kunal Vyas[5]

David S. Tuch[6]

Alan Britten[7]

Mieke Van Hemelrijck[1]

Gary J. Cook[8]

Chris Sibley-Allen[9]

Sarah Allen[9]

Arnie Purushotham[1,2]

Running title: CLI for assessing breast tumor margins

Author affiliations:

[1] – King's College London, Division of Cancer Studies, London, UK;

[2] – Department of Breast Surgery, Guy's and St Thomas' NHS Foundation Trust, □London, UK;

[3] – Anesthetic Department, Guy's and St Thomas' NHS Foundation Trust, □London, UK;

[4] – Day Surgery Unit, Guy's and St Thomas' NHS Foundation Trust, □London, UK;

[5] – Sagentia Ltd., Cambridge, UK;

[6] – Lightpoint Medical Ltd., Chesham, UK;

[7] – Medical Physics Department, St George's Hospital, London, UK;

[8] – King's College London, Division of Imaging Sciences and Biomedical Engineering, London, UK

[9] – Department of Nuclear Medicine, Guy's and St Thomas' NHS Foundation Trust, □London, UK;

Conflicts of interest: David S. Tuch is an employee of and a shareholder in Lightpoint Medical Ltd. The other authors have no conflicts of interest to disclose.

Corresponding author

Name: Arnie Purushotham

Address: Department of Research Oncology, 3rd Floor Bermondsey Wing, Guy's Hospital, SE1 9RT, London

Phone: +44 (0) 207 188 3027

Email: arniepurushotham@gmail.com

First author

Name: Maarten Grootendorst (PhD student)

Address: Department of Research Oncology, 3rd Floor Bermondsey Wing, Guy's Hospital, SE1 9RT, London

Phone: +44 (0) 75 188 92692

Email: maarten.grootendorst@kcl.ac.uk

Word count: 6922

ABSTRACT

Rationale: In early-stage breast cancer, the primary treatment option for the majority of women is breast-conserving surgery (BCS). There is a clear need for more accurate techniques to assess resection margins intraoperatively, as on average 20% of patients require further surgery to achieve clear margins. Cerenkov luminescence imaging (CLI) combines optical and molecular imaging by detecting light emitted by 18F-fluorodeoxyglucose (^{18}F-FDG). Its high-resolution and small size imaging equipment makes CLI a promising technology for intraoperative margin assessment. A first-in-human study was conducted to evaluate the feasibility of ^{18}F-FDG CLI for intraoperative assessment of tumor margins in BCS.

Methods: Twenty-two patients with invasive breast cancer received 5 MBq/kg ^{18}F-FDG 45-60 min prior to surgery. Sentinel lymph node biopsy (SLNB) was performed using an increased technetium-99m (^{99m}Tc)-nanocolloid activity of 150 MBq to facilitate nodal detection against the gamma-probe background signal (cross-talk) from ^{18}F-FDG. The cross-talk and ^{99m}Tc dose required was evaluated in two lead-in studies. Immediately after excision, specimens were imaged intraoperatively in an investigational CLI imaging system. The first 10 patients were used to optimize the imaging protocol; the remaining 12 patients were included in the analysis dataset. CLI images from incised BCS specimens were analyzed postoperatively by two surgeons blinded to the histopathology results, and mean radiance and margin distance were measured. Agreement between margin distance on CLI and histopathology was assessed. Radiation doses to staff were measured.

Results: Ten of the 12 patients had an elevated tumor radiance on CLI. Mean radiance and tumor-to-background ratio were 560 ± 160 photons/s/cm^2/sr and 2.41 ± 0.54, respectively. All 15 assessable margins were clear on CLI and histopathology. Agreement in margin distance and inter-rater agreement was good (κ = 0.81 and 0.912, respectively). Sentinel lymph nodes (SLNs) were successfully detected in all patients. Radiation dose to staff was low; surgeons received a mean dose of 34 ± 15 μSv per procedure.

Conclusions: Intraoperative ^{18}F-FDG CLI is a promising, low-risk technique for intraoperative assessment of tumor margins in breast-conserving surgery. A randomized controlled trial will evaluate the impact of this technique on re-excision rates.

Key words: Cerenkov luminescence imaging; breast-conserving surgery; tumor margins; ^{18}F-FDG; sentinel lymph node biopsy

INTRODUCTION

In early-stage breast cancer, the primary treatment option for the majority of women is BCS by wide local excision (WLE) of the tumor. WLE often fails to achieve clear surgical margins, and on average 20% of patients who undergo BCS will require repeat surgery to achieve clear margins (*1*) (although this may vary since there is no global agreement of the definition of 'clear margins'). Re-operations potentially have several negative consequences including delayed commencement of adjuvant therapy, worse cosmesis, increased patient anxiety and costs (*2,3*).

There have been several attempts to assess surgical margins intraoperatively in order to reduce breast cancer re-operation rates post-WLE (*1*). Techniques evaluated to date include specimen radiography, intraoperative ultrasound, touch imprint cytology, frozen section, and radiofrequency spectroscopy. However, these all have limitations in terms of adequate performance, practicality and/or cost-effectiveness (*1*). Experimental methods evaluated include Raman spectroscopy, ambient mass spectrometry, optical coherence tomography, diffuse reflectance spectroscopy, confocal microscopy, and (targeted) fluorescence imaging (*1*). Each of these techniques have unique limitations, and the diagnostic performance remains to be evaluated in large-scale studies.

Positron emission tomography (PET) using ^{18}F-FDG is a powerful tool for *in vivo* imaging of breast cancer. While whole-body PET has limited diagnostic sensitivity for primary breast cancer, high-resolution PET imaging with positron emission mammography has shown high sensitivity (92-96%) and specificity (84-91%) for breast cancer diagnosis (*4-6*). Intraoperative high-resolution imaging of ^{18}F-FDG could therefore provide a powerful tool for surgical guidance. However, intraoperative PET is impractical due to the large size and expense of a PET scanner and PET's low spatial resolution. Development of a compact, high-resolution, intraoperative PET scanner could address these limitations.

Recently, it has been discovered that PET imaging agents emit optical photons via a phenomenon called Cerenkov luminescence (*7*). Cerenkov photons are generated by positrons travelling at super-relativistic speeds in tissue. Optical imaging of Cerenkov photons emitted by PET agents is an emerging imaging modality called CLI. CLI combines high diagnostic performance and clinical translatability of PET imaging with high spatial resolution and compactness of optical cameras, thus making it a promising technology for intraoperative margin assessment in breast cancer surgery (*8*).

In this first-in-human clinical trial we evaluated the feasibility, safety, and preliminary performance of ^{18}F-FDG CLI using a novel intraoperative CLI camera to assess tumor margin status in breast cancer patients undergoing WLE with SLNB or with axillary lymph node dissection (ALND).

MATERIALS AND METHODS

Intraoperative ^{18}F-FDG CLI in breast-conserving surgery

Patient recruitment and patient preparation on the day of surgery. Research Ethics Committee approval was obtained prior to patient recruitment (ClinicalTrials.gov identifier NCT02037269). Between June 2014 and February 2016, patients with histologically confirmed invasive breast cancer on core biopsy with or without associated ductal carcinoma in situ (DCIS), due to undergo primary BCS and SLNB or ALND, were recruited at Guy's Hospital in London after written informed consent was obtained. Exclusion criteria were: age <30 years, previous surgery or radiotherapy to the ipsilateral breast in the preceding two years, neoadjuvant systemic therapy, pregnancy or lactation, blood glucose level of ≥12 mmol/l on the day of surgery and known hypersensitivity to ^{18}F-FDG. Females of childbearing age required a negative pregnancy test (by beta HCG qualitative analysis), history of surgical sterilization, or history of amenorrhea in the past twelve months. □

On the day of surgery patients scheduled to undergo SLNB received a periareolar intradermal injection of 150 MBq ^{99m}Tc-albumin-nanocolloid (Nanocoll^{TM}, GE Healthcare, UK). The increased ^{99m}Tc activity of 150 MBq was calculated based on the results from two lead-in cross-talk studies (Supplemental Material). Patients were then injected intravenously with 5 MBq/kg ^{18}F-FDG (up to a maximum of 300 MBq) and typically 45-60 min post-^{18}F-FDG injection were taken to the operating theatre.

Surgery and intraoperative specimen radiography. Following induction of anesthesia, patients due to undergo SLNB received a periareolar subdermal injection of 2ml Patent Blue V and 3ml of normal saline. To minimize radiation exposure to theatre staff by reducing the time spent in close proximity to the patient, a standard breast operating set was pre-arranged on a sterile tray. Surgery to the breast was performed ahead of SLNB/ALND to minimize signal intensity reduction from radiotracer decay in the time between

^{18}F-FDG injection and CLI imaging. The WLE specimen was excised using monopolar diathermy (Valleylab Force FX[TM] electrosurgical generator with HCP-01 Skintact surgical pencil). The excised specimen was orientated with sutures and metal surgical clips as per local protocol.

Post-excision WLE specimens were x-rayed intraoperatively (Faxitron Bioptics, USA), and excision of cavity shave margins was performed if the tumor was deemed to be close to the edge of the specimen on radiography.

Following excision of the WLE specimen, SLNB or ALND was performed. For SLNB a Europrobe 3 gamma probe with a high-energy collimator was used (Eurorad SA, France). SLNs were defined as nodes that were radioactive, blue, or palpable (9). The number of excised SLNs, the *ex vivo* SLN gamma probe signal (counts per second), and the presence of blue nodal discoloration were recorded. Upon completion of the procedure the gamma probe background signal in the axilla was measured.

Intraoperative CLI of WLE specimens and lymph nodes. Following specimen radiography, CLI imaging of the WLE specimen was performed using an investigational intraoperative CLI imaging system (Lightpoint Medical Ltd, UK). This system consists of a custom-built light-tight dark box containing two optical pathways: one for CLI and one for white-light imaging for anatomic reference (Fig. 1A). The CLI imaging pathway includes a fast f/.95 lens and a reflex mirror to fold the optical pathway into an electron-multiplying charge coupled device (EMCCD) camera. The field-of-view of the CLI camera is 8×8 cm, and the acquisition matrix is 512×512 to give a pixel resolution of 156.25 μm. The EMCCD is thermoelectrically-cooled to -80°C and radiation-shielded with lead to prevent annihilation photons from scintillating in the EMCCD chip, i.e. "gamma strikes". The white-light imaging pathway provides a photographic reference image using a standard complementary metal-oxide-semiconductor camera.

The WLE specimen was positioned on a specimen table (Fig. 1B), the margin of interest placed in the center of the field-of-view by using the surgical sutures to guide orientation, and subsequently imaged.

Following intact WLE specimen imaging, the surface of the specimen was immediately inked intraoperatively in order to preserve its orientation for histopathological analysis (Supplemental Material Fig. 1A). Six distinct ink colors (Davidson[®], Bradley Products Inc., USA) were applied to the six margins. The inked specimen was then incised through the posterior margin to visualize the primary tumor and

tumor margins, and the incised WLE specimen was imaged (Supplemental Material Figs. 1B and 1C). In one patient sequential image acquisition over a 50-minute time-period was performed to determine the half-life ($t_{1/2}$) of the radiance observed in the tumor.

The first 10 patients were included in the optimization dataset and the remaining 12 patients in the analysis dataset. In the first 10 patients, the image acquisition protocol was optimized by testing different image acquisition times (100, 300, 400 sec) and pixel binning settings (2x2, 4x4, 8x8). A 300-sec acquisition time and 8x8 pixel binning was found to provide sufficient sensitivity for tumor detection and acceptable spatial resolution (1.25 mm) within a time-window feasible for intraoperative use, and these setting were used in the remaining 12 patients included in the analysis dataset. Upon completion of WLE CLI, the activity of the WLE specimen was estimated using a scintillation monitor (Type 41/44A, ThermoScientific, USA) or handheld radiation spectrometer (Raymon10 GR1, Kromek PLC). SLNs were also imaged intraoperatively with CLI using the same imaging settings.

After imaging was completed, WLE specimens were sent for histopathological analysis as per standard practice.

Radiation safety monitoring. Radiation safety monitoring was performed to ensure safe working practices were maintained and that work was compliant with UK legislation regarding ionizing radiation (*10-12*). Prior to commencing the study all staff received training to become familiar with radiation control procedures, occupational risks, and learned how to minimize exposure without compromising patient care. Staff members were issued with electronic personal radiation dose monitors (PDM-112 and PDM-122, Hitachi-Aloka Medical Ltd., Japan) for the body, and thermo-stimulated luminescent ring dosimeters for extremities (Landauer, UK). Radiation contamination monitoring of staff, rooms, equipment and waste was carried out after each procedure using a scintillation monitor (Type 41/44A, Series 300 mini-monitor, ThermoScientific, USA). As ^{99m}Tc has a longer half-life (6.02 hours) than [18]F (110 min) the radioactive waste storage requirements for CLI procedures are similar to standard SLNB procedures. The time taken for the various stages of the procedure, i.e. from induction of anesthesia to recovery, were recorded.

Histopathology. Histopathological analysis was performed as per UK National guidelines: the WLE specimen was sliced at 2 mm intervals, and representative sections of the tumor and all 6 relevant margins were selected by the pathologist, processed, paraffin wax embedded and 3 to 4 micron sections were cut and stained with hematoxylin and eosin. Microscopic margin distance measurements were performed by a Consultant breast pathologist (S.E.P.). Microscopic invasive tumor size and whole tumor size (including DCIS extending from the main invasive mass) were also measured. Positive margins were defined as invasive cancer or DCIS <1 mm from the specimen surface. The histological margin distances were reported in increments of 1 mm, but margins more than 5 mm were reported as >5 mm. The pathologist was blinded to the interpretation of the CLI images.

Image analysis. All CLI and radiography images were analyzed postoperatively in order to provide a controlled and standardized analysis environment. Measurements of the mean radiance (photons/s/cm^2/sr) were performed by drawing region-of-interests on the unprocessed CLI images. Region-of-interests were selected in areas showing increased signal intensity ('tumor') and no increased signal ('tissue background'). Tumor-to-background ratios (TBRs) were calculated. Gamma strikes were excluded from region-of-interest analysis. The tumor radiance from the sequential incised WLE images was fit to a monoexponential, to determine the radiance half-life.

Assessment of margin status on CLI was performed on the incised WLE specimen images. The analysis was done independently by two experienced breast surgeons (AP and AK), and performed prior to analysis of the radiography images to prevent potential confirmation bias from *a priori* knowledge of the radiological margin status. Prior to analysis CLI images were processed by applying a median filter (filter size range 5 – 10, filter threshold range 10 – 15) and Gaussian filter (filter width: 1, filter threshold: 0.5). A stronger Gaussian filter (filter width: 4 or 5) was applied to images with a low TBR to increase the visibility of the tumor. The preoperative diagnostic information that would typically be available to the surgeon was provided including patient age, clinical, mammographic and ultrasound tumor size, screen detected (Y/N), and histological tumor type, grade and receptor status on core biopsy. Per patient, a color image containing information on specimen orientation was shown together with a grey-scale image and Cerenkov image. All images were displayed on a standard computer monitor (23", 1920 x 1080 pixels,

250 cd/m^2 luminance). The grey-scale image was overlaid with the Cerenkov signal to provide a fused image containing both functional and anatomical information. The leveling was set using the software's default leveling, and manually adjusted based on the surgeon's clinical judgment. Both surgeons then independently reported whether an elevated radiance from the tumor could be identified on CLI; in patients displaying an elevated tumor radiance the margin distance of the margins visible in the image was measured using the ruler function in the imaging software (Mirada XD3, Mirada Medical, Oxford, UK). The total time required to complete margin assessment was approximately 2 min per patient. As an exploratory outcome measure, tumor size was also measured. Upon completion of the measurements surgeons were asked whether, given the CLI image, they would have performed a cavity shaving had the image been available at the time of surgery. Surgeons also scored image quality on a 5-point Likert scale: 1 = very poor – image not interpretable, 2 = poor but interpretable, 3 = fair, 4 = good, 5 = very good.

Following CLI image analysis, specimen radiography image analysis was performed on a Coronis 3MP screen (20.8", 1536 x 2048 pixels, 500 cd/m^2 luminance) using standard GE PACS imaging software. Surgeons were presented with the same preoperative diagnostic information, but the images were shown in a different order to avoid potential sequential bias. The number of surgical marker clips was noted, and the reliability of specimen orientation assessed. If the orientation was considered reliable, the margin distance and tumor size on radiography was measured. Whether an additional cavity shaving would have been performed based on the radiography image was also noted.

The final histopathology results of the surgically excised tissue were not available at the time of CLI and radiography image analysis, and could therefore not bias the surgeon's assessment.

Statistics. Weighted Kappa coefficients were calculated to assess the agreement in margin distance between CLI and definitive histopathology, and to assess the inter-rater agreement between surgeons ('irr' package, version 3.2.2, R statistical software). A kappa coefficient (κ) greater than 0.75 was considered good agreement (*13*). Agreement between histological tumor size and tumor size on CLI and radiography respectively was assessed by calculating the mean difference in tumor size ± std, and intraclass correlation coefficients (ICC) (SPSS® version 23.0; IBM, Chicago).

RESULTS

Intraoperative imaging of WLE specimens

A total of 22 patients were included in the study. The CLI results and postoperative histopathology results from the 12 patients included in the analysis dataset are shown in Table 1. The mean administered ^{18}F-FDG activity was 295 ± 18 MBq (range 259 – 325). The mean time between ^{18}F-FDG injection and WLE excision was 86 ± 26 min (range 50 – 146), and the mean time between ^{18}F-FDG injection and commencement of CLI image acquisition was 118 ± 26 min (range 88 – 180).

Tumor margin assessment was performed on incised WLE specimen images to allow for visualization of the tumor extent and to avoid image artifacts created by the monopolar diathermy. Ten of the 12 patients in the analysis dataset had elevated tumor radiance on CLI (Table 1). Mean tumor radiance and TBR in these 10 patients was 560 ± 160 photons/s/cm^2/sr (range 308 – 871) and 2.41 ± 0.54 (range 1.63 – 3.22). The half-life of the tumor radiance was 115.5 min, which is consistent with the 109.8-minute half-life of ^{18}F. This concordance supports that the detected tumor radiance is Cerenkov luminescence from ^{18}F-FDG. Mean radioactivity in the WLE specimen at the time of CLI imaging was 90 ± 48 kBq in patients with an elevated radiance; in the 2 patients without an elevated radiance radioactivity was 14 kBq and 19 kBq, respectively.

In the 10 patients with elevated tumor radiance, a total of 60 margins could be assessed histologically, 26 margins were evaluable on specimen radiography, and 15 margins were assessable on CLI. Of the 45 histological margins that were not evaluable on CLI, 40 were not in the field-of-view of the CLI image, and 5 could not be assessed due to migration of the specimen orientation ink onto the margin edge, preventing optical margin interrogation. Eighteen of the 60 histological margins were not assessable on specimen radiography due to the inability to reliably orientate the specimen on the radiography image, and 16 margins were not in the image field-of-view.

The margin distance from the 15 margins as measured on CLI and histopathology is shown in Table 1. Two margins measured between 1 and 5 mm on CLI and histopathology (Figs. 2 and 3); the remaining 13 margins were >5 mm by both modalities. There was good agreement between the histological margin distance and the margin distance on CLI as measured by both surgeon 1 and surgeon

2, respectively (κ surgeon 1 = 0.76, κ surgeon 2 = 0.86). The agreement in margin distance between surgeons was also good (κ = 0.91).

Five margins could be assessed on both CLI and specimen radiography, and all were >5 mm on both modalities, as well as histologically. An example of a CLI, radiography and histopathology image from a patient with >5 mm resection margin widths is shown in Fig. 4.

Two patients (17%) had a positive margin on postoperative histopathological analysis; both were medial margins with DCIS <1 mm distant. These margins were not visible in the CLI image as specimen incision had only exposed the superior, inferior and posterior margins; the medial margin could therefore not be assessed.

In 8 of the 10 patients tumor size could be measured on CLI, and compared to histopathology: the agreement is shown in Table 1. In 2 patients the orientation inks prevented measurement of tumor size on CLI. Invasive tumor size showed excellent agreement; mean difference for both surgeons combined was -0.84 ± 2.8 mm. ICC was 0.84 and 0.81 for surgeons 1 and 2, respectively. Whole tumor size was underestimated on CLI; mean difference for both surgeons combined was -4.7 ± 5.0 mm. ICC was 0.65 and 0.69 for surgeons 1 and 2, respectively. Inter-rater agreement between surgeons was excellent (ICC = 0.97).

The agreement between invasive tumor size on histopathology and on radiography was good; mean difference for both surgeons combined was 1.0 ± 3.1 mm. ICC was 0.56 and 0.58 for surgeons 1 and 2, respectively. Whole tumor size was underestimated on radiography; mean difference for both surgeons combined was -5.2 ± 8.9 mm.

CLI image quality in the 10 patients with successful CLI was scored as 4.3 (range 4 – 5) by both surgeons.

Sentinel lymph node detection and ^{18}F-FDG Cerenkov lymph node imaging

SLNB was performed in 21 of the 22 patients; 1 patient underwent an ALND. SLNs were successfully identified in all 21 patients. A total of 43 SLNs were removed. The average number of SLNs per patient was 2 (range 1 – 4). Two of the 21 SLNB patients had macrometastatic SLNs.

The mean gamma probe signal of the 'hottest' SLN per patient was 4991 ± 2521 counts per second (range 8500 – 170). The mean gamma probe signal of the 'second hottest' SLN was 2505 ± 2632 counts per second (range 7368 – 50). Mean axillary background signal, measured in 13 patients, was 192 ± 70 counts per second (range 55 – 270). This signal is lower than the ^{18}F-FDG gamma probe cross-talk measured in the lead-in study (Supplemental Material), and is mainly due to the longer time between ^{18}F-FDG injection and SLNB (mean 93 ± 34 min). A total of 7 nodes had a gamma probe signal below the background signal; 6 of these were blue. This indicates the importance of using the combined technique of radioisotope and blue dye in ^{18}F-FDG CLI guided breast surgery, as low-uptake nodes may be missed if gamma probe detection is used alone.

All SLNB procedures were performed with the monopolar diathermy device and due to the observed image artifact from diathermy on CLI, the SLN images were uninterpretable.

Radiation dose to staff

A summary of the whole body effective radiation dose to primary personnel from all 22 procedures is shown in Table 2. Surgeons received the highest mean and maximum dose of 34 µSv and 74 µSv respectively. Mean duration of surgery was 39 ± 11 min (range 21 – 61) during which the surgeon was generally <0.5 meters from the patient. Mean radiation dose to the left and right hand of the surgeon was 126 ± 95 µSv (0 – 250) and 78 ± 75 µSv (0 – 200), respectively. Mean and maximum radiation dose received by the anesthetist standing at approximately 1 meter from the patient, with closer patient contact at the time of induction of anesthesia and at the end of the procedure, was 11 µSv and 18 µSv, respectively. Surgical equipment had low levels of radioactive contamination, which was undetectable 1-3 days later. No staff members were found to be contaminated with radioactivity after the procedures.

DISCUSSION

This first-in-human study evaluated the feasibility of intraoperative ^{18}F-FDG CLI for assessing tumor margin status in patients with invasive breast cancer undergoing BCS, and SLNB or ALND. Tumor margin assessment on CLI could be performed in 10 of the 12 patients in the analysis dataset, and there was strong agreement between CLI and definitive histopathology on margin width. An exploratory outcome

measure assessed the correlation between tumor size on CLI and histopathology; the size on CLI and histopathology correlated well for invasive cancer, while whole tumor size (invasive with associated DCIS) was underestimated on CLI. Results from the radiation monitoring program demonstrated that the procedure can be carried out safely while maintaining low radiation exposures to the staff involved.

In 2 patients margin assessment could not be performed because the tumors did not display elevated radiance on CLI. The absence of signal in these patients is probably due to the small tumor size, a factor known to be associated with lower ^{18}F-FDG uptake (14), and the late time points at which these tumors were imaged (135 min and 180 min post ^{18}F-FDG injection; the first and third longest injection-imaging time of all patients). Unsuccessful CLI imaging due to the absence of a detectable tumor signal highlights the importance of ongoing developments focused on improving detection sensitivity of camera systems to aid detection of tumors with low ^{18}F-FDG uptake including lower grade tumors and DCIS (4).

Since its discovery in 2009, CLI has rapidly emerged as a powerful technique for cancer imaging. CLI is readily translatable to the clinic due to existing regulatory approval and widespread availability of PET imaging agents (15). In contrast, targeted fluorescence imaging requires prohibitive clinical development times and capital investment for regulatory and reimbursement approval of novel imaging drugs (16). Three clinical pilot studies of CLI have been published to date. These have focused on the use of CLI to image radiopharmaceutical uptake in the thyroid, CLI for non-invasive detection of nodal disease, and Cerenkov luminescence endoscopy to aid detection of cancerous lesions in the GI tract (17-19). To our knowledge, this is the first report of intraoperative CLI. Its high-resolution, small size imaging equipment and minute-scale image acquisition (5 min) and image analysis (~2 min) times, make CLI of particular interest for image-guided surgery. The feasibility of intraoperative CLI as shown in this study in combination with the wide applicability of ^{18}F-FDG across a range of solid cancers provides a stepping stone for clinical evaluation of this technology in other cancer types.

The low radiation exposure to staff found in this study is in accordance with previously reported exposure levels from ^{18}F-FDG guided breast surgery procedures (20,21), and comparable to the radiation dose reported for interventional cardiology procedures (1 – 50 µSv) (22). The number of ^{18}F-FDG CLI-guided BCS procedures that could be performed in a routine clinical setting depends on the occupational limits on radiation exposure per country (Table 2). In the UK and US the occupational annual dose limit is

20 mSv (*23*) and 50 mSv (*24*), respectively. Good practice would dictate that the radiation exposure from a procedure should be kept As Low As Reasonable Achievable, i.e. well below the dose limits. In practice in the UK, if a worker is likely to receive annually more than 6mSv they would be designated a classified worker, necessitating annual medical surveillance and longer term record keeping of their radiation exposure.

Image artifacts on CLI from tissue excised with the monopolar diathermy device prevented tumor margin assessment on intact WLE specimens and assessment of SLNs. Although the source of this 'false-signal' is not yet fully understood, current evidence from pre-clinical experiments points towards long-lived, thermally-induced chemiluminescence (*25*). Since the emission seems to be related to temperature, which can reach up to 250°C at the tip of the diathermy device, electrosurgical devices that operate at much lower temperatures are currently being tested (*26*). In addition to potentially facilitating margin assessment on intact WLE specimens, an advantage of low-temperature devices over monopolar diathermy is the reduced collateral tissue damage, which could also improve the accuracy of assessing tumor resection margins on histopathology (*27*).

Although CLI imaging of incised WLE specimens is feasible for assessing tumor margin status, this approach has some limitations over margin assessment on intact specimens. Firstly, migration of the wet pathology ink onto the margin edge immediately after specimen incision hinders margin interpretation with CLI. Methods to accelerate drying of inks by applying acetic acid to the painted tissue or by using fast drying inks may be solutions to this problem, but this has not been tested in this study. Secondly, in our institution specimen incision could only be performed through the posterior margin to ensure accurate postoperative histological assessment of radial margins. Consequently, only a limited number of margins could be assessed with CLI imaging per patient, and two histologically positive margins that were not visible in the CLI image were therefore missed. In order to assess more margins per patient specimen incision may be performed in multiple planes, but good communication between surgeons and pathologists is paramount in order to not compromise patient care.

A randomized, controlled, multi-center clinical study is scheduled to commence in late 2016 to evaluate the effect of intraoperative ^{18}F-FDG CLI on re-operation rate and Quality of Life in BCS (ClinicalTrials.gov identifier NCT02666079). The study will run across an anticipated 8 study sites in the

UK and Germany and use the CE-marked LightPath^{TM} Imaging System (Lightpoint Medical Ltd, UK). The smaller field-of-view of 6 x 6 cm and improved imaging software may provide substantial improvements in sensitivity over the investigational CLI camera used in the present study. By analyzing larger subgroups of patients with a range of tumor types (including DCIS), size, histological grades and hormone receptor status, further insight should be obtained into which breast-cancer patient populations may most benefit from CLI-guided surgery.

CONCLUSION

Intraoperative ^{18}F-FDG CLI in BCS for invasive breast carcinoma is a promising and low-risk procedure. CLI imaging of incised WLE specimens provides high-resolution functional information that allows surgeons to accurately assess margin status with good correlation to gold-standard histopathological examination. Further work, focused on suppressing the optical signal from the monopolar diathermy device, will assist margin assessment on intact WLE specimens and potentially identification of SLN metastases on CLI. SLNB can be performed successfully during ^{18}F-FDG CLI-guided surgery by using 150 MBq ^{99m}Tc-nanocolloid and blue dye. Based on the results of this study a larger randomized controlled study is warranted to evaluate the impact of intraoperative ^{18}F-FDG on re-operation rate and Quality of Life in BCS.

DISCLOSURES

ACKNOWLEDGEMENTS

REFERENCES

1. St John ER, Al-Khudairi R, Ashrafian H, et al. Diagnostic Accuracy of Intraoperative Techniques for Margin Assessment in Breast Cancer Surgery: A Meta-analysis. *Ann Surg.* 2016.

2. Munshi A, Kakkar S, Bhutani R, Jalali R, Budrukkar A, Dinshaw KA. Factors influencing cosmetic outcome in breast conservation. *Clin Oncol (R Coll Radiol).* 2009;21:285-293.

3. Abe SE, Hill JS, Han Y, et al. Margin re-excision and local recurrence in invasive breast cancer: A cost analysis using a decision tree model. *J Surg Oncol.* 2015;112:443-448.

4. Kalinyak JE, Berg WA, Schilling K, Madsen KS, Narayanan D, Tartar M. Breast cancer detection using high-resolution breast PET compared to whole-body PET or PET/CT. *Eur J Nucl Med Mol Imaging.* 2014;41:260-275.

5. Narayanan D, Madsen KS, Kalinyak JE, Berg WA. Interpretation of positron emission mammography and MRI by experienced breast imaging radiologists: performance and observer reproducibility. *AJR Am J Roentgenol.* 2011;196:971-981.

6. Schilling K, Narayanan D, Kalinyak JE, et al. Positron emission mammography in breast cancer presurgical planning: comparisons with magnetic resonance imaging. *Eur J Nucl Med Mol Imaging.* 2011;38:23-36.

7. Das S, Thorek DL, Grimm J. Cerenkov imaging. *Adv Cancer Res.* 2014;124:213-234.

8. Grootendorst MR, Cariati M, Kothari A, Tuch DS, Purushotham A. Cerenkov luminescence imaging (CLI) for image-guided cancer surgery. *Clinical and Translational Imaging.* 2016:1-14.

9. Mansel RE, MacNeill F, Horgan K, et al. Results of a national training programme in sentinel lymph node biopsy for breast cancer. *Br J Surg.* 2013;100:654-661.

10. The ionising radiations regulations 1999. No. 3232.: Health and Safety Executive; 1999.

11. Ionising radiation (medical exposure) regulations 2000 (IRMER). Department of Health; 2012.

12. The environmental permitting (England and Wales) regulations 2010. Department for environment, food and rural affairs; 2010.

13. Khan KS, Chien PF. Evaluation of a clinical test. I: assessment of reliability. *BJOG.* 2001;108:562-567.

14. Kumar R, Chauhan A, Zhuang H, Chandra P, Schnall M, Alavi A. Clinicopathologic factors associated with false negative FDG-PET in primary breast cancer. *Breast Cancer Res Treat.* 2006;98:267-274.

15. Spinelli AE, Boschi F. Novel biomedical applications of Cerenkov radiation and radioluminescence imaging. *Phys Med.* 2015;31:120-129.

16. Agdeppa ED, Spilker ME. A review of imaging agent development. *AAPS J.* 2009;11:286-299.

17. Spinelli AE, Ferdeghini M, Cavedon C, et al. First human Cerenkography. *J Biomed Opt.* 2013;18:20502.

18. Thorek DL, Riedl CC, Grimm J. Clinical Cerenkov luminescence imaging of (18)F-FDG. *J Nucl Med.* 2014;55:95-98.

19.   Hu H, Cao X, Kang F, et al. Feasibility study of novel endoscopic Cerenkov luminescence imaging system in detecting and quantifying gastrointestinal disease: first human results. *Eur Radiol.* 2015;25:1814-1822.

20.   Heckathorne E, Dimock C, Dahlbom M. Radiation dose to surgical staff from positron-emitter-based localization and radiosurgery of tumors. *Health Phys.* 2008;95:220-226.

21.   Andersen PA, Chakera AH, Klausen TL, et al. Radiation exposure to surgical staff during F-18-FDG-guided cancer surgery. *Eur J Nucl Med Mol Imaging.* 2008;35:624-629.

22.   Duran A, Hian SK, Miller DL, Le Heron J, Padovani R, Vano E. Recommendations for occupational radiation protection in interventional cardiology. *Catheter Cardiovasc Interv.* 2013;82:29-42.

23.   The 2007 recommendations of the international commission on radiological protection. ICRP publication 103. Ann. ICRP 37 (2-4). International Commission on Radiological Protection; 2007.

24.   USNRC. Standards for protection against radiation. 10 CFR 20.1201.

25.   Sun JS, Tsuang YH, Chen IJ, Huang WC, Hang YS, Lu FJ. An ultra-weak chemiluminescence study on oxidative stress in rabbits following acute thermal injury. *Burns.* 1998;24:225-231.

26.   Loh SA, Carlson GA, Chang EI, Huang E, Palanker D, Gurtner GC. Comparative healing of surgical incisions created by the PEAK PlasmaBlade, conventional electrosurgery, and a scalpel. *Plast Reconstr Surg.* 2009;124:1849-1859.

27.   Ruidiaz ME, Cortes-Mateos MJ, Sandoval S, et al. Quantitative comparison of surgical margin histology following excision with traditional electrosurgery and a low-thermal-injury dissection device. *J Surg Oncol.* 2011;104:746-754.
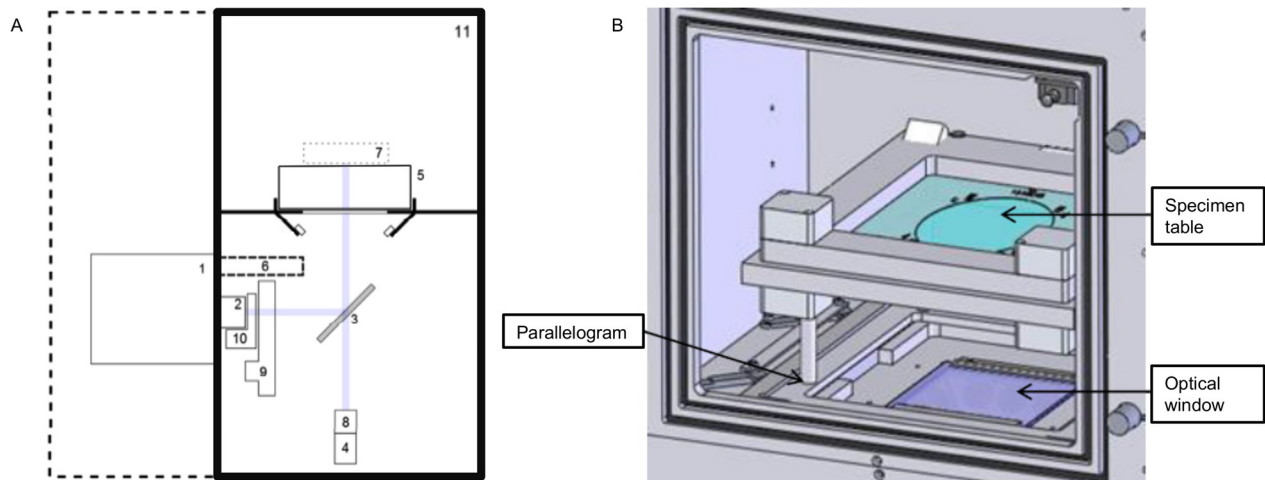
Figure 1: Investigational intraoperative CLI specimen camera. (A) Schematic diagram. Component labels: 1) EMCCD camera, 2) f/.95 lens, 3) Hinged reflex mirror, 4) Complementary metal-oxide-semiconductor reference camera, 5) Specimen table, 6) Lead radiation shielding for EMCCD camera, 7) Focal zone, 8) Fixed lens for reference camera, 9) Filter wheel, 10) LED RGB light array, 11) Specimen chamber. The purple line shows the optical paths for the EMCCD camera and the reference camera as determined by the angle of the reflex mirror. (B) Specimen chamber. The specimen table is placed on a parallelogram to facilitate accurate positioning of the specimen in the center of the image.
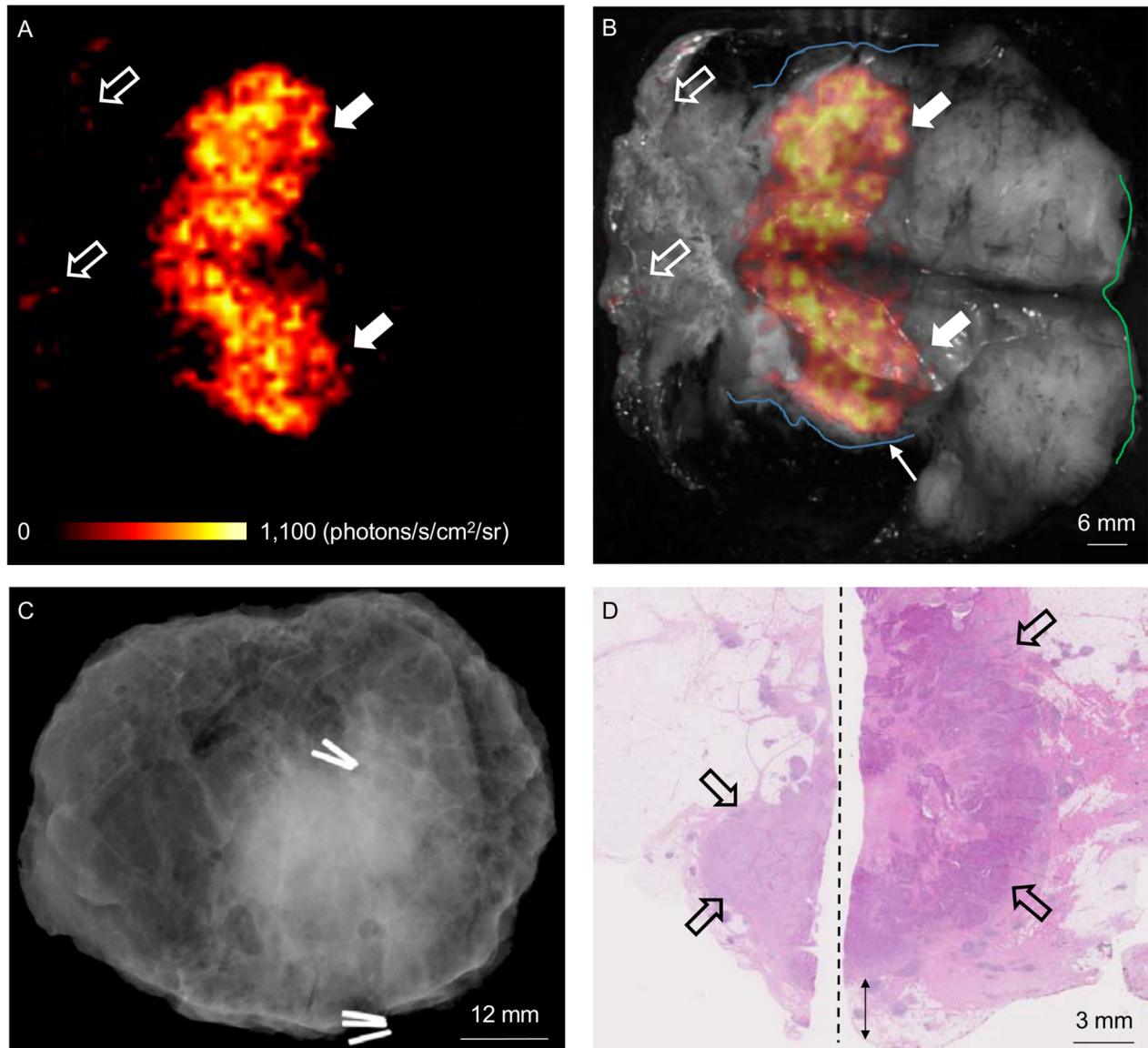
Figure 2: WLE specimen from a patient with a grade 3, ER-/HER2-, no special type (NST) carcinoma. (A) Cerenkov image; (B) Grey-scale photographic image overlaid with Cerenkov signal. An increased signal from the tumor is visible (white arrows); mean radiance is 871 ± 131 photons/s/cm^2/sr, mean TBR is 3.22. Both surgeons measured the posterior margin (outlined in blue) as 2 mm (small arrow); a cavity shaving would have been performed if the image had been available intraoperatively. The medial margin (outlined in green) measured >5 mm by both surgeons. Pathology ink prevented assessing the lateral margin; a phosphorescent signal is visible (open arrows). (C) Specimen radiography image. The absence of one surgical clip to mark the anterior margin, and the odd position of the superior margin clip (white arrow) prevented reliable margin assessment. (D) Combined histopathology image from two adjacent pathology slides on which the posterior margin (bottom of image) and part of the primary tumor are visible (open arrows). The distance from the posterior margin measured 3 mm microscopically (double arrow). The medial margin is > 5 mm (not present in image).
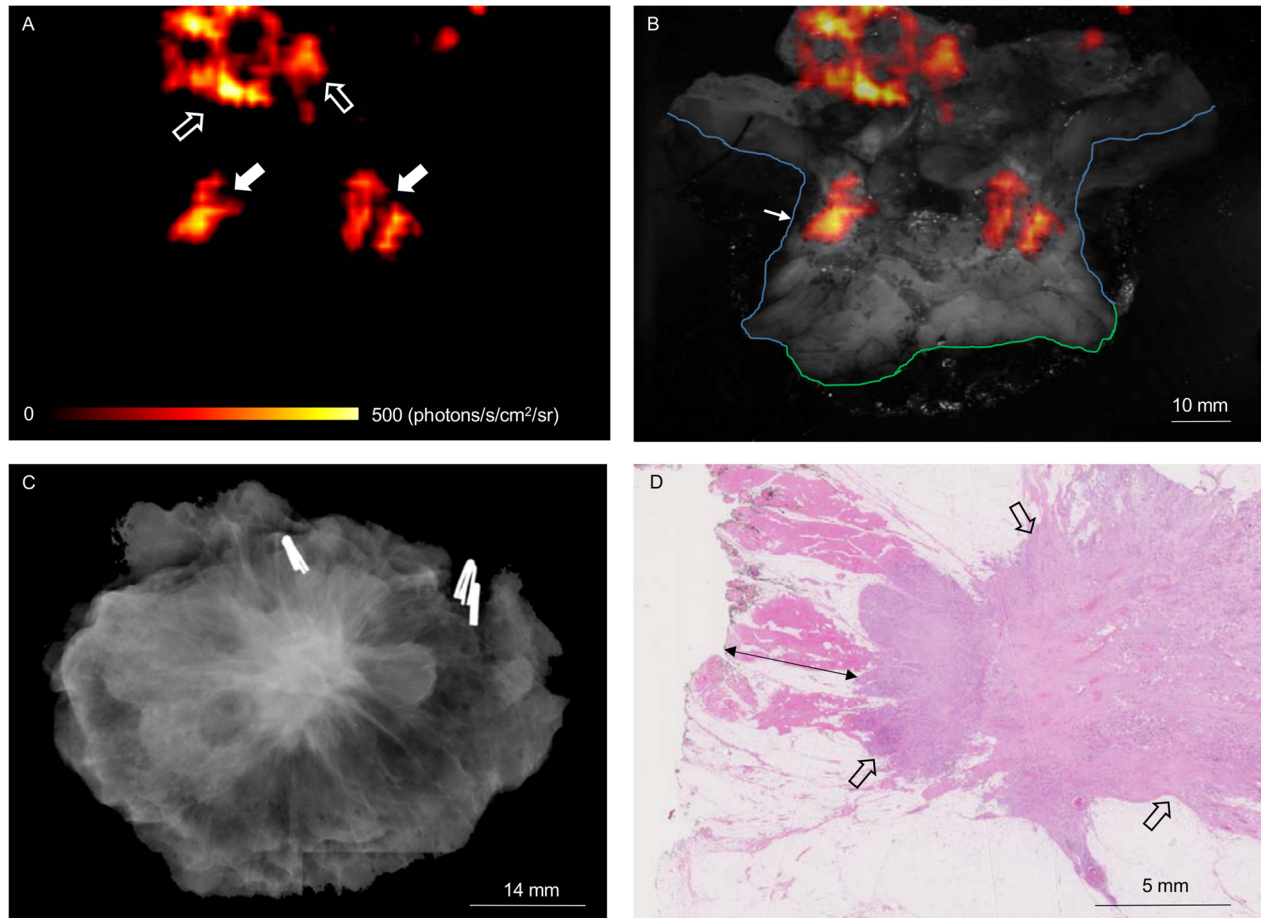
Figure 3: WLE specimen from a patient with a grade 3, ER+/HER2-, NST carcinoma admixed with high grade DCIS. (A) Cerenkov image; (B) Grey-scale photographic image overlaid with Cerenkov signal. An increased signal from the tumor is visible (white arrows); mean radiance is 406 ± 51 photons/s/cm^2/sr, mean TBR is 2.03. The posterior margin (outlined in blue) is 2 mm or 3 mm on CLI as measured by surgeons 1 and surgeon 2, respectively; both surgeons would have performed a cavity shaving. The medial margin (outlined in green) is >5 mm. (C) Specimen radiography image. All 4 radial margins were >5 mm, and both surgeons indicated they would not have performed a cavity shaving. (D) Histopathology image showing the posterior margin (left side of image) and part of the tumor (open arrows). The posterior margin was 5 mm distant histologically (double arrow).
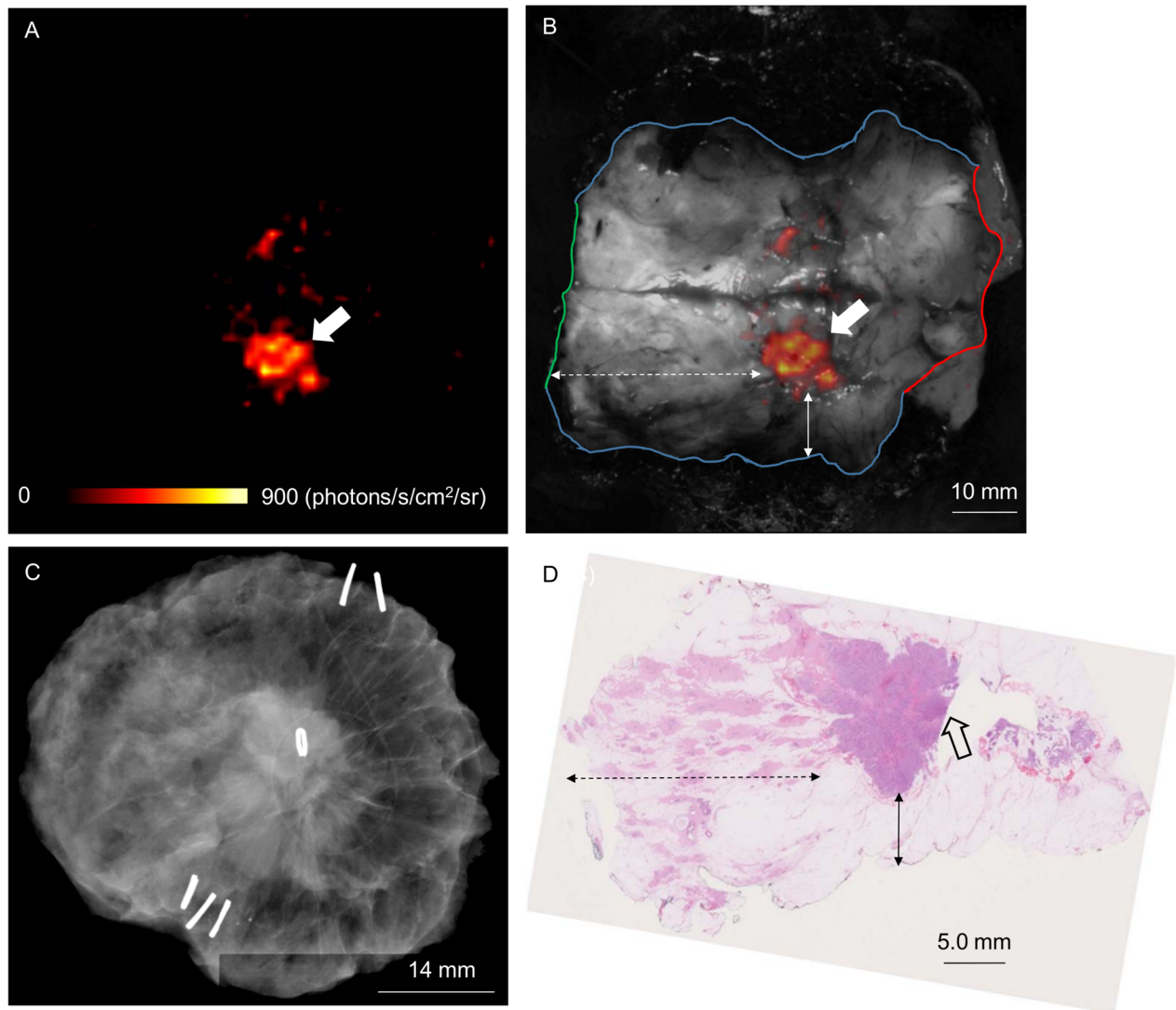
Figure 4: WLE specimen from a patient with a grade 3, ER+/HER2-, NST carcinoma admixed with high grade DCIS. (A) Cerenkov image; (B) Grey-scale photographic image overlaid with Cerenkov signal. An elevated signal (white arrow) from the tumor can be seen. Mean radiance is 637 ± 47 photons/s/cm^2/sr; mean TBR is 1.63. Both surgeons measured the posterior margin (outlined in blue), medial margin (outlined in green) and lateral margin (outlined in red) distances as >5 mm; a cavity shaving would not have been performed based on the CLI image. (C) Specimen radiography image. All 4 radial margins were >5 mm as measured by both surgeons and did not prompt resection of cavity shave margins (D) Histopathology image from large-format pathology block. The tumor is >5 mm from the posterior margin (solid arrow), medial margin (dashed arrow) and lateral margin (not visible in image).

Table 1: CLI and postoperative histopathology results for each patient in the analysis dataset.

Patient	Tumor type[1]	Histologic grade invasive (1 – 3)	ER/HER2 status of invasive cancer (Pos/Neg)[2]	Mean tumor radiance (photons/s/cm2/sr)	TBR[3]	Margin distance CLI surgeon 1, 2[7] (mm)	Margin distance histopath[5] (mm)	Tumor size CLI surgeon 1, 2[7] (mm)	Invasive tumor size histopath[8] (mm)	Whole tumor size histopath[8] (mm)
1	NST DCIS	2	Pos/Neg	-[4]	-	-	-	-	13	13
2	NST DCIS	3	Neg/Pos	453.59	2.34	6, 6	>5	*[6]	22	22
3	NST	3	Neg/Neg	871.16	3.22	2, 2 28, 30	3 >5	20, 18	20	20
4	NST DCIS	3	Neg/Neg	-[4]	-	-	-	-	14	14
5	NST DCIS	3	Pos/Neg	405.76	2.03	2, 3	5	18, 18	20	20
6	ILC	2	Pos/Neg	544.04	2.44	9, 9	>5	20, 19	22	22
7	NST	3	Pos/Neg	667.47	2.72	10, 11	>5	*[6]	25	25
8	NST DCIS	2	Pos/Neg	308.30	1.63	6, 8 16, 15	>5 >5	19,19	15	35
9	NST DCIS	3	Pos/Neg	593.93	3.08	14, 13 6, 7	>5 >5	14, 15	18	19
10	NST DCIS	3	Pos/Neg	648.29	2.46	8, 8	>5	22, 22	19	29
11	NST DCIS	2	Pos/Neg	466.03	2.54	15, 14	>5	13, 11	13	13
12	NST DCIS	3	Pos/Neg	637.08	1.63	9, 9 30, 31 22, 22	>5 >5 >5	12, 10	14	14

1. *NST: invasive carcinoma of ductal/no special type, DCIS: ductal carcinoma in situ, ILC: invasive lobular carcinoma*
2. *Pos: positive, Neg: negative*
3. *Tumor-to-background ratio*
4. *No elevated tumor radiance on CLI*
5. *Histopath: histopathology*
6. *Presence of orientation inks prevented measuring tumor size on CLI.*
7. *Margin distance and tumor size are shown for surgeon 1 and 2, respectively*
8. *The histopathological tumor size displayed in the table is the tumor size measured in the same direction as the tumor size measurement on CLI. In patient 3, 11 and 12 the largest invasive and whole tumor size (i.e. extent of DCIS and invasive cancer) was measured in a different direction, and was 32 mm, 33 mm and 12 mm, respectively*

Table 2: Measured effective radiation doses by occupation from 22 surgical procedures.

Staff Group	N[1]	Mean Effective Dose per procedure ± std (µSv)	Range (µSv)	Estimated number of procedures per individual per year[2] ICRP[3] (20 mSv annual limit)	Estimated number of procedures per individual per year[2] USNRC[4] (50 mSv annual limit)
Surgeon	46	34 ± 15	8 – 74	270	676
Anesthetist	22	11 ± 5	0 – 18	1111	2778
NM technologist	22	9 ± 4	1 – 15	1333	3333
Anesthetist assistant	22	6 ± 3	0 – 11	1818	4545
Trial Co-coordinator	21	5 ± 2	1 – 10	2000	5000
Recovery Nurse	43	4 ± 3	0 – 14	1429	3571
Scrub Nurse	22	2 ± 1	0 – 5	4000	10000
Periphery Nurse	23	1 ± 1	0 – 4	5000	12500
Research fellow	36	1 ± 2	0 – 13	1538	3846
Ward Nurse	15	0	0 – 1	20000	50000
Tissue Biobank Practitioner	14	0	0 – 1	20000	50000

1. *N = number of measurements*
2. *Based on maximum Effective Dose per procedure per staff group*
3. *ICRP: International Commission on Radiological Protection*
4. *USNRC: United States Nuclear Regulatory Commission*

SUPPLEMENTAL MATERIAL

METHODS

Standard practice requires the use of [99mTc]–labeled radiopharmaceuticals for SLNB. The presence of [18F]-FDG in study subjects results in greater than normal background signal being detected by the handheld gamma probe used for SLNB, due to the down-scatter of 511keV Fluorine-18 ([18F]) gamma photons into the [99mTc] energy window. This cross-talk background could potentially hinder detection of low-activity SLNs. To assess the [18F] cross-talk and to determine the activity of [99mTc]-nanocolloid required to successfully perform standard of care SLNB in patients undergoing [18F]-FDG CLI-guided surgery, two lead-in studies were conducted prior to commencing the CLI study.

Lead-in study I: SLNB simulations using the GAPS simulator

To determine the effects of the cross-talk background on the detectability of radioactive lymph nodes a simulation study was performed using the computerized gamma probe simulator (GAPS) (*1*). The GAPS system has previously been used in the UK national breast SLNB training program 'NEW START', and provides simulations of the radioactivity distribution and gamma probe response that allows accurate objective assessment of the surgeon's ability to localize SLNs on the surface of a manikin of the female breast and axilla.

The aim of the study was to measure the accuracy of gamma probe guided localization of nodes with varying levels of radioactivity and varying levels of cross-talk background.

The measurements were performed by two breast surgeons (AP and AK), with extensive experience of performing SLNB procedures. After one test case to familiarize the surgeons with the GAPS system, each surgeon was presented with 3 simulated SLNB cases individually. In each case the injection site, two SLNs and a spatially uniform [18F] background signal with Poisson distributed noise were simulated. The simulated SLN count rates ranged between 56 and 373 counts per second, and were based on a 150MBq [99mTc] injection, a SLN tracer uptake ranging from 0.06% to 0.4% of the administered dose, an average SLN depth (30mm from the axillary skin surface) (*2*), and a time between tracer injection and SLN detection of 3 hours, which is common for 1-day SLNB protocols. The dose of 150MBq [99mTc] is markedly higher than the standard dose of 20MBq used for 1-day SLNB procedures at Guy's Hospital. This increased dose was chosen to ensure a significant rise in SLN

count rate, thus facilitating SLN detection in a ^{18}F background, whilst keeping within a dose range that is well established (*3*). The range in SLN % tracer uptake covers the lower spectrum of tracer uptake reported in literature (*4*), thus assessing the surgeon's performance in the clinically most challenging situation of identifying SLNs with a low count rate. The ^{18}F background signal was set to a mean of 560 cps, corresponding to an ^{18}F-FDG dose of 5MBq/kg, which is the dose CLI study patients received. Calibration measurements of count rates from ^{99m}Tc and ^{18}F sources with the same gamma probe system and high-energy collimator as in the CLI study, the Europrobe 3 (Eurorad S.A., France), were used to set the count rates simulated by the GAPS system. The signal-to-noise ratio, defined as the ratio of the node count rate to the background count rate, varied from 0.67 and 0.10 in the simulations.

The surgeons performed surface scans with the GAPS gamma probe to localize as many nodes as they could, and to indicate when they thought they had localized a SLN. SLN detection was only considered successful if the surgeon indicated that they had located a node and if the position pointed at by the probe was within 10mm of the virtual node.

Lead-in study II: Gamma probe measurements in 18F-FDG PET patients

Following on from the SLNB simulations, gamma probe measurements of the axilla were performed in patients scheduled for a diagnostic ^{18}F-FDG PET scan to confirm that the simulated ^{18}F background signal corresponded to the gamma probe cross-talk found *in vivo*.

After research ethics committee approval and written informed consent was obtained, a total of 20 female patients were included at the PET Centre at St Thomas's Hospital (ISRCTN29552671). Approximately 60 minutes after receiving an intravenous injection of ^{18}F-FDG, but prior to PET imaging, the Europrobe 3 gamma probe with a high energy collimator was used to perform 10 second measurements of the lowest and highest count rates in the left and right axilla, respectively. The measurements of both axillae were performed shortly after each other (within 5 minutes) so that effects of radioactive decay between measurements were negligible. The background count rate was also measured, and the 10s count rates were averaged to give cps. The gamma probe system and configurations used to perform the ^{18}F-FDG axillary cross-talk measurements were the same as in the CLI study. The axilla was defined as the triangle between the pectoralis major, the latissimus dorsi and the edge of the breast. By placing the probe perpendicular to the skin, the entire axilla was scanned.

Patient and injection characteristics such as height, weight and injected activity were recorded. An independent samples t-test was performed to compare the highest signal in the right axilla and left axilla respectively, and a p-value of <0.05 was considered statistically significant.

RESULTS

### Lead-in study I: SLNB simulations using the GAPS simulator

The SLN detection results per surgeon can be found in Supplemental Table 1. The majority of the SLNs were accurately detected. Nodes with 0.4% (373 cps), 0.3% (280 cps) and 0.1% (93 cps) of injected activity were found by both surgeons, representing successful localization of nodes even with a signal-to-noise ratio as low as 0.17. Both surgeons missed the SLN with the lowest simulated uptake (0.06% uptake, 56 cps). The mean spatial accuracy for detected nodes was 2.6mm and 4.0mm for surgeon 1 and surgeon 2, respectively.

Lead-in study II: Gamma probe measurements in ^{18}F-FDG PET patients

The patient and ^{18}F-FDG injection characteristics can be found in Supplemental Table 2. The mean and standard deviation of the lowest and highest gamma probe signal in the right axilla was 310 ± 77 cps (range 133 – 488) and 372 ± 85 cps (range 233 – 616), respectively. The mean and standard deviation of the lowest and highest gamma probe signal in the left axilla was 299 ± 80 cps (range 161 – 553) and 359 ± 74 cps (range 236 – 582), respectively. These mean values are lower than the 560cps (5MBq/kg) used in the SLNB simulations, which were obtained from gamma probe calibration measurements with ^{18}F distributed in a water volume. The lower values probably reflect the renal excretion and non-uniform uptake *in vivo*. The highest count rate, which is clinically most relevant as it causes the greatest interference when detecting SLNs, did not differ between left and right axilla (p = 0.596), thus indicating that the cross-talk is similar in both axillae.

Based on the findings from both lead-in studies the investigators were confident that by using an increased administered activity of 150 MBq ^{99m}Tc-nanocolloid, a gamma probe collimator suitable for 511 keV energy photons and blue dye, SLNB could be performed safely and successfully, and patient recruitment to the CLI study commenced.

FIGURES FOR SUPPLEMENTAL MATERIAL
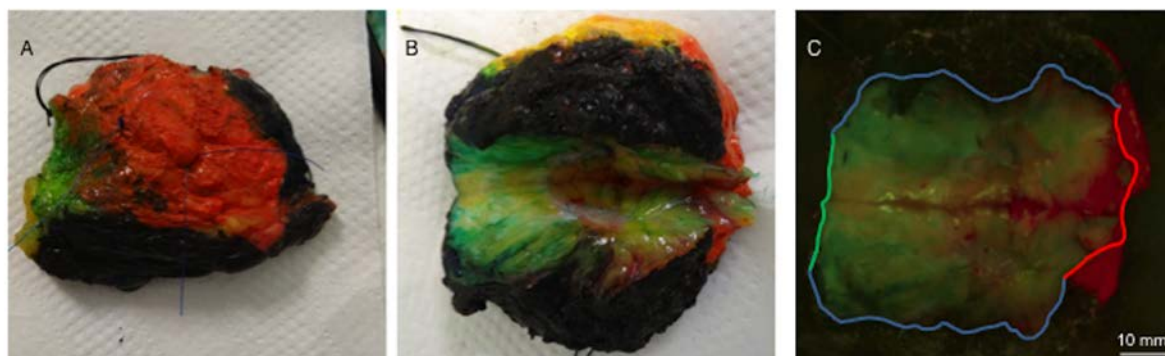
Supplemental Figure 1: Intraoperative inking and incising of WLE specimen. (A) Inks and sutures were applied to the WLE specimen to aid anatomical specimen orientation. (B) WLE specimen following initial incision through the posterior (black) margin, exposing the primary tumor and margins of excision. (C) White-light image of incised WLE specimen obtained with the CLI imaging system. Compared to (B) the specimen was further incised and opened to maximize the visibility of the posterior margin (outlined in blue), medial margin (outlined in green) and lateral margin (outlined in red). This image was used to assess tumor margins on CLI (Fig. 4B in manuscript).

TABLES FOR SUPPLEMENTAL MATERIAL

Supplemental Table 1: SLN detection results from SLNB simulations using the GAPS simulator.

Surgeon	Case	^{18}F BG[1] (cps)[2]	SLN 1 (cps)	SLN 1 detected?	Localization error SLN 1 (mm)	SLN 2 (cps)	SLN 2 detected?	Localization error SLN 2 (mm)
1	1	560	373	Y	2.50	93	Y	6.40
	2	560	280	Y	1.40	93	Y	2.43
	3	560	280	Y	0.50	56	N	-
2	1	560	373	Y	1.27	93	Y	3.99
	2	560	280	Y	3.00	93	Y	9.70
	3	560	280	Y	2.00	56	N	-

1. *BG = background signal*
2. *CPS = counts per second*

Supplemental Table 2: Patient and ^{18}F-FDG injection characteristics from the gamma probe cross-talk study in PET patients.

Characteristic	Mean (range)
Age (years)	61.5 (40-81)
Height (cm)	161 (145-178)
Weight (kg)	69.3 (45-101)
Blood glucose level (mmol/L)	5.7 (4.3-16.4)
Injected Activity (MBq)	343.8 (307.5-387.0)
Time between injection and first measurement (min)	59.7 (49-79)

REFERENCES FOR SUPPLEMENTAL MATERIAL

1.　　Britten A, Newey VR, Clarke R. A computerized gamma probe simulator to train surgeons in the localization of sentinel nodes. *Nucl Med Commun.* 2007;28:225-229.

2.　　Mathelin C, Salvador S, Huss D, Guyonnet JL. Precise localization of sentinel lymph nodes and estimation of their depth using a prototype intraoperative mini gamma-camera in patients with breast cancer. *J Nucl Med.* 2007;48:623-629.

3.　　Giammarile F, Alazraki N, Aarsvold JN, et al. The EANM and SNMMI practice guideline for lymphoscintigraphy and sentinel node localization in breast cancer. *Eur J Nucl Med Mol Imaging.* 2013;40:1932-1947.

4.　　Rubello D, Zavagno G, Bozza F, et al. Analysis of technical and clinical variables affecting sentinel node localization in patients with breast cancer after a single intradermal injection of 99mTc nanocolloidal albumin. *Nucl Med Commun.* 2004;25:1119-1124.